A CONSERVATIVE INTERFACE SHARPENING LATTICE BOLTZMANN MODEL

T. REIS[†]

Abstract. A lattice Boltzmann model for the propagation and sharpening of phase boundaries that arise in applications such as multiphase flow is presented. The sharpening is accomplished through an artificial compression term that acts in the vicinity of the interface and in the direction of its surface normal. This term is embedded into the moments of the two-relaxation-time discrete velocity Boltzmann partial differential equation, which is discretized in space and time to yield a second order algorithm. Stringent one- and two-dimensional tests for sharp propagating fronts are performed. The proposed model is shown to conserve the phase field to machine precision and allows narrow interfaces to advect correctly with the flow field with minimal lattice pinning and facetting.

Key words. lattice Boltzmann, sharp interfaces, pinning, multiphase flow, TRT, artificial compression

1. Introduction. Multiphase flow problems with propagating interfaces are encountered in many important engineering applications, particularly in the oil industry. It is often the case that the width of an interface between fluids is orders of magnitudes smaller than other length scales of the flow and thus is modelled as a discontinuity or a very thin transition region in the flow. Numerical simulations of these models are performed most efficiently on fixed Eulerian grids but the accurate representation of propagating interfaces that are vanishingly narrow on a macroscopic scale is still a major challenge of computational fluid dynamics (CFD). Interfacial flows involve multiple time and length scales, causing significant difficulties for conventional interface-capturing techniques. Volume of Fluid methods [7, 18] advect the volume fraction of fluid in a cell and the interface is then approximated by straight lines through the cells or fitted by piecewise linear interface construction (PILC) methods [52]. They may also include antidiffusive operators to reduce numerical diffusion and maintain narrow interfaces [45]. Volume of Fluid approaches conserve mass but cannot naturally handle significant changes in topology. Level set methods on the other hand [42, 33, 43] can efficiently compute interface deformations such as cusps but require a reinitialization routine to improve mass conservation [41]. Alternatively, diffuse-interface models [2] introduce an order parameter, ϕ, that undergoes a rapid but smooth variation in the interfacial region. Phase field models may be obtained from physical considerations of the internal structure of interfaces and thus can be used to study flow on the scale of the physical transition region. Diffuse interface models can also be used for numerical convenience to simulate multiphase flow at much larger length scales. Computations using these models usually predict an interface that is smeared over many grid points and hence many times larger than its actual (physical)

Funding: The author's work was supported by the UK Consortium on Mesoscopic Engineering Science (UKCOMES) [grant EP/L00030X/1].

[†]School of Computing and Mathematical Sciences, University of Greenwich, London, SE10 9LS, UK (T.Reis@greenwich.ac.uk).

width. To predict accurate results while making the most of spatial resolution it is desirable to make this boundary between phases as narrow as possible, usually by introducing interface sharpening terms or routines into the numerical algorithm. Folch et al. [9] added a "counter term" to eliminate curvature effects at leading order in the phase field model, allowing interface motion to be driven by advection only. Sun and Beckermann [47] developed general interface capturing methods for sharp interfaces based on the phase-field approach and the counter term proposed by Folch et al. and Chiapolino, Saurel, and Nkonga [5] introduced a specific flux limiter to counteract the numerical diffusion that can cause excessive smearing in diffuse interface models, while Tiwari, Freund, and Pantano [49] proposed an interface regularization approach for maintaining reasonable narrow phase boundaries in compressible multiphase flows. Olsson, Kreiss, and Zahedi [32] developed a modified reinitialization step for multiphase level set methods that maintains sharp interfaces and reported that their algorithm maintains narrow interfaces and demonstrates excellent convergence and conservation properties. Although not originally motivated by, or applied to, diffuse interface models, the method of Olsson, Kreiss, and Zahedi [32] includes a diffusive term to improve numerical stability. Their method is inspired by the Artificial Compression Method for contact discontinuities of Harten [16], which reduces the smearing of shocks and maintains their resolution in finite difference methods. Since in multiple-dimensional multiphase flows the artificial compression flux, $\mathbf{F}(\phi)$, should act in the direction of the interface normal $\mathbf{n}$, and only on regions where the level set function ϕ is in the range $0 < \phi < 1$, Olsson, Kreiss, and Zahedi [32] used $\mathbf{F}(\phi) = \phi(1-\phi)\mathbf{n}$ to reinitialize the level set and counteract the diffusion.

Since its original development, the lattice Boltzmann method (LBM) has been extended to a large number of application areas, one of the more promising being that of multiphase flow simulations in porous media (see, for example, [20, 31, 1, 40, 51, 19, 50, 25, 35]). The LBM is a numerical algorithm derived from a velocity-space truncation of the Boltzmann equation that is most commonly used to simulate fluid flow. The basic structure of the algorithm—a linear advection operator and a local algebraic collision operator—lends itself to high-end parallel processing and has allowed for computations in highly irregular geometries. Thus it is no surprise that the application of the LBM to multiphase flow in porous media has received a lot of attention. The multiphase LBMs that already exist in the literature are usually categorized as follows: Color gradient models, which are based on Rothman and Keller's original Lattice Gas Cellular Automaton (LGCA) approach [39, 12, 11, 38]; Shan and Chen [44] pseudo-molecular interaction models [4]; and free-energy models [48, 36, 22] which incorporate Cahn–Hilliard theories for phase separation. Similar to free-energy models are the modern LBMs for nonideal gasses of He, Chen, and Zhang [17] and their advancements by Lee and Fischer [26] and Lee and Lin [27]. All types of multiphase LBMs have been applied to problems where the lengthscale of phase transition is vanishingly small compared to other lengthscales of the flow but all predict diffuse interfaces that are many times wider than what is physically realistic. The color gradient type models compute narrower interfaces than the other models but attempting to minimize their width causes spurious phenomena, most notability lattice pinning, where the interface fails to advect correctly. This means it moves slower than the flow advection speed, sometimes not moving at all, with the development of planar segments (facetting) in multiple dimensions. That is, the interface becomes pinned to the underlying computational grid.

The problem of lattice pinning has previously been reported by Latva-Kokko and Rothman [24], Halliday, Hollis, and Care [14], and Reis and Dellar [37]. Halliday,

Hollis, and Care [14] noticed that interfaces computed with the model proposed by Lishchuk, Care, and Halliday [30], which incorporates surface tension effects via an additional interfacial body forcing term, has a tendency to facet and pin at low capillary and low drop Reynolds numbers. This is attributed to the spurious microcurrents surrounding a droplet, which are a result of numerical errors in calculating gradients of a phase field (which is evaluated using finite differences) when the interface is sharp. Latva-Kokko and Rothman [24] argue that pinning is not necessarily related to the presence of spurious currents. In [24] the authors give evidence of pinning when the parameter controlling surface tension is set to zero, and hence free from anisotropic pressure gradients and microcurrents. Therefore, Latva-Kokko and Rothman [24] conclude that pinning in color gradient models is purely an artefact of the color redistribution algorithm that is necessarily employed to maintain sharp boundaries between fluids. Both articles attempt to eliminate pinning in their respective models: Halliday, Hollis, and Care [14] propose using both a body force consistent with the approach of Guo, Zheng, and Shi [13] together with a higher order scheme for the calculation of the spatial derivatives of the phase field; while Latva-Kokko and Rothman [24] suggest using a modified, less severe, recoloring step. In the sense that pinning diminishes in a given parameter range, both groups present positive conclusions regarding their modified approaches. However, pinning was still evident outside of this range, and any noticeable improvement came at the price of wider interfaces (and greater computational expense in [14]). The segregation step of Latva-Kokko and Rothman [24] has been used in conjunction with the multicomponent LBM of Halliday et al. [15] and in a range of values of the segregation parameter ($\beta < 0.7$) the combined model allows a circular drop of fluid to advect in a surrounding fluid of equal density without pinning or any noticeable anisotropy. However, an instability arises for larger values of β (sharper interfaces). Spencer and Halliday [46], on the other hand, used a low order interpolation method to compute approximations to interface discontinuities with a phase field multicomponent lattice Boltzmann model, while other authors have preferred to develop front-tracking LBMs [23].

Reis and Dellar [37] noticed that this spurious behavior is similar to that observed in the numerical simulation of hyperbolic partial differential equations coupled to stiff source terms [29, 8, 34]. By "stiff" we mean the timescale T associated with the source term is much shorter than the timestep, Δt, one would naturally use for the advective part of the equation. These equations are common in application areas such as nonequilibrium gas dynamics, combustion, and chemically reacting flows, which typically involve a scalar field ϕ representing, for example, the fraction of unburnt fuel. The lengthscale of transition from $\phi \sim 0$ to $\phi \sim 1$ is assumed to be vanishingly thin in the Chapman–Jouguet theory of combustion, just like phase boundaries in macroscopic descriptions of multiphase flow. Colella, Majda, and Roytburd [8] documented the structure and dynamical stability of reacting shock layers by numerically solving the equations for a compressible, chemically reacting gas using fractional step schemes. By fully resolving the shock layer they were able to corroborate the complex behavior of the reacting shock profiles as the heat release varies. On larger spatial scales it is practical to compute on a coarser mesh. For moderately fine meshes Colella, Majda, and Roytburd [8] report a serious defect with high order Godunov methods for reacting gases in the shock wave regime: "*The numerical wave structure has a discrete weak detonation profile moving at the mesh speed—one grid per time step—with all chemical energy released in this numerical precursor wave following by a slower moving shock wave.*" LeVeque and Yee [29] investigated the misbehavior of numerical solutions of stiff PDEs using a model problem with a still algebraic source

(reaction) term (this is discussed briefly in section 2). In the underresolved case, their numerical results predict the discontinuity to either move at the incorrect speed of one grid point per timestep or to not move at all. This is what is observed in lattice pinning. Pember [34] further investigated the issue of incorrect propagation speed of fronts and states necessary conditions to avoid spurious solutions.

Reis and Dellar [37] developed a lattice Boltzmann formulation of the model problem of LeVeque and Yee [29] to better understand lattice pinning. They provided an explanation of pinning in terms of the disparity of timescales between diffusion and interface sharpening and, following the ideas of Bao and Jin [3], showed that introducing a quasi-random sharpening threshold can greatly delay the onset of pinning. However, to conserve volume in multidimensional flows, the model proposed by Reis and Dellar [37] required an integration over the fluid domain at each time step. This introduces an additional computational burden. Furthermore, the approach does not readily lend itself to flows with significant local changes in interface topology and thus may not be appropriate for some realistic engineering flows.

In this article we propose a new lattice Boltzmann algorithm for sharpening interfaces. By casting a sharpening term in diffusive form, based on the artificial compression of Olsson, Kreiss, and Zahedi [32], and building it into the moments of the discrete velocity Boltzmann partial differential equation, we develop an LBM for interface sharpening that is second order accurate in space and time and conserves mass organically. The computational price to pay is need for some (nonlocal) numerical differentiation on the lattice, but this is required in *all* multiphase LBMs. The resulting numerical scheme is nevertheless simple, accurate, does not leak mass, and can capture significant interface deformations.

The remainder of this article is structured as follows. In section 2 we discuss the problem of stiffness in more detail and summarize the LBM model of Reis and Dellar [37] that is based on LeVeque and Yee's [29] model problem for hyperbolic PDEs with stiff source terms. In section 3 we construct the conservative sharpening term, show the connection between LeVeque and Yee's source terms and the Artificial Compression of Olsson, Kreiss, and Zahedi [32], and present the conservative Boltzmann sharpening model. Numerical simulations of stringent test problems are performed in section 4 before making concluding remarks in section 5.

2. Stiffness and pinning. To try and understand the misbehavior of numerical solutions to stiff partial differential equations, LeVeque and Yee studied the following model problem:

$$\phi_t + u\partial_x\phi = S(\phi) = \frac{1}{T}\,\phi\,(1-\phi)(\phi-\tfrac{1}{2}), \tag{2.1}$$

where $\phi \in [0,1]$ is a scalar field representing, for example, the different fluid phases. The left-hand side of (2.1) describes advection while the source term $S(\phi)$ on the right-hand side is a phase field sharpening term. We see that $S(\phi)$ has three equilibrium points, the two stable ones of $\phi = 0$ and $\phi = 1$, and the unstable (or critical) one of $\phi = 1/2$. Thus the source term is a sharpener that drives all points where $\phi > \frac{1}{2}$ back towards $\phi = 1$, and all points where $\phi < \frac{1}{2}$ back towards $\phi = 0$ over a fast time scale T. The numerical difficulty with computing this equation is the timescale T is typically orders of magnitude smaller than the natural advection timestep Δt one would use in a numerical solver. One must usually resolve the fastest scale to predict reasonable results. Of course it is more desirable to use a scheme that will allow for larger timesteps, and hence more efficient computing, such as a splitting method.

Using a splitting technique, LeVeque and Yee [29] showed that smooth but physically meaningless results could be computed. In particular, they found that, starting from initial conditions representing a step transition from $\phi = 0$ to $\phi = 1$, the discontinuity either propagated with the incorrect speed of one grid point per timestep or did not move at all, depending on the Courant number.

Reis and Dellar [37] developed a lattice Boltzmann formulation of (2.1) to understand pinning in multiphase LBMs. They postulated the discrete Boltzmann equation

$$\partial_t f_i + c_{i\alpha}\,\partial_\alpha f_i = -\frac{1}{\tau}\left(f_i - f_i^{(0)}\right) + R_i, \tag{2.2}$$

where $f_i^{(0)}$ is the equilibrium function

$$f_i^{(0)} = W_i\phi\left(1 + \frac{1}{\lambda}c_{i\alpha}u_\alpha\right), \tag{2.3}$$

and R_i is the term responsible for sharpening. In the above, u_α is the advection velocity (which is assumed to be constant) and $\{c_{i\alpha}|i = 1, \ldots b\}$ are a given set of discrete particle velocities that form an integer lattice, such as the D2Q9 lattice shown in Figure 1. Throughout this paper we use the convection of using Latin subscripts to refer to the direction of particle velocity and Greek subscripts to refer to Cartesian components of a vector. The W_i in the equilibria (2.3) are constant weights associated with the lattice velocities $c_{i\alpha}$ and

$$\lambda\delta_{\alpha\beta} = \sum_i W_i c_{i\alpha}c_{i\beta}, \tag{2.4}$$

where $\delta_{\alpha\beta}$ is the Kronecker delta function.

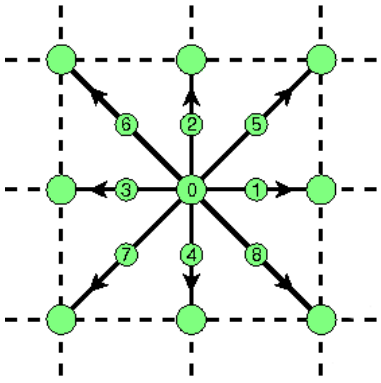

FIG. 1. *The D2Q9 lattice. The numbers on the lattice links refer to the subscript i of the discrete particle velocities $\mathbf{c}_i$.*

The advection-diffusion-reaction equation is embedded in the discrete velocity Boltzmann equation (see (2.2)), with the phase field ϕ defined to be the zeroth moment of f_i,

$$\phi = \sum_i f_i. \tag{2.5}$$

To furnish the model (2.1) in the macroscopic limit, the sharpening term is required to fulfill

$$\sum_i R_i = S(\phi), \quad \sum_i R_i c_{i\alpha} = u_\alpha S(\phi). \tag{2.6}$$

Taking the first two moments of (2.2) with respect to the particle velocities yields

$$\partial_t \phi + \partial_\alpha \psi_\alpha = S(\phi), \tag{2.7}$$

$$\partial_t \psi_\alpha + \partial_\beta \Pi_{\alpha\beta} = -\tfrac{1}{\tau}\left(\psi_\alpha - \psi_\alpha^{(0)}\right) + u_\alpha S(\phi), \tag{2.8}$$

respectively, where

$$\psi_\alpha = \sum_i f_i c_{i\alpha}, \quad \Pi_{\alpha\beta} = \sum_i f_i c_{i\alpha} c_{i\beta}. \tag{2.9}$$

As is standard in the lattice Boltzmann approach, the target equation ((2.1) in this case) is found by seeking slowly varying solutions of (2.2). An expansion of $\boldsymbol{\psi}$, $\boldsymbol{\Pi}$, and the temporal derivatives ∂_t in powers of the collision time τ,

$$\psi_\alpha = \psi_\alpha^{(0)} + \tau\psi_\alpha^{(1)} + \cdots, \quad \Pi_{\alpha\beta} = \Pi_{\alpha\beta}^{(0)} + \tau\Pi_{\alpha\beta}^{(1)} + \cdots, \quad \partial_t = \partial_{t_0} + \tau\partial_{t_1} + \cdots \tag{2.10}$$

allows us to find the equilibrium contributions to the first two nonconserved moments,

$$\psi_\alpha^{(0)} = \sum_i f_i^{(0)} c_{i\alpha} = \phi u_\alpha, \quad \Pi_{\alpha\beta}^{(0)} = \sum_i f_i^{(0)} c_{i\alpha} c_{i\beta} = \lambda\phi\delta_{\alpha\beta} \tag{2.11}$$

and the first correction to the flux

$$\psi_\alpha^{(1)} = -\left(\lambda\delta_{\alpha\beta} + u_\alpha u_\beta\right)\partial_\beta \phi. \tag{2.12}$$

Thus one obtains from the discrete velocity Boltzmann equation (2.2) the advection-diffusion-reaction equation (see [37] for full details)

$$\frac{\partial\phi}{\partial t} + \mathbf{u}\cdot\nabla\phi = S(\phi) + \tau\lambda\nabla^2\phi + \mathcal{O}\left(u^2\right). \tag{2.13}$$

The leading order terms match the desired equation (2.1). The inevitable diffusive correction term at $\mathcal{O}(\tau)$ sets the width of the transition region between $\phi = 0$ and $\phi = 1$. Reis and Dellar [37] reduced the model (2.2) to fully discrete form to obtain a lattice Boltzmann algorithm (see subsection 3.2) and showed that lattice pinning occurs when the ratio τ/T is large, that is, when we try to minimize the width of phase boundaries.

To overcome the numerical difficulties of pinning, Reis and Dellar [37] took inspiration from a random projection method for hyperbolic conservation laws coupled with stiff source terms proposed by Bao and Jin [3]. Bao and Jin [3] modelled the effect of the sharpening term by an explicit projection of the phase field to an equilibrium solution at each timestep. However, rather than the direction of the projection being determined by some fixed critical value (e.g., $\phi_c = 1/2$, as in $S(\phi)$), they introduce a random threshold that remains fixed in space but varies from timestep to timestep. By taking this threshold to be an element from the van der Corput sequence they were able to predict the correct average propagation speed of a sharp interface over many timesteps. We note that, unlike Chorin's random choice method [6] which

uses a generalized Riemann solver for the advection, the random projection method uses a random variable only in the stiff source term. For a lattice Boltzmann random projection method, Reis and Dellar [37] replaced the unstable equilibrium point of $1/2$ in the source term $S(\phi)$ in their lattice Boltzmann with a random threshold, ϕ_c, taking from the van der Corput sequence, whose average is $\langle \phi_c \rangle = 1/2$. They showed that their approach allowed very sharp phase boundaries to propagate correctly in one dimension. In multiple dimensions, the sharpening term causes the phase field volume to decrease when the interfaces have curvature unless a reinitialization step that involves a integration over the domain to find a mass-conserving ϕ_c at each time step is introduced. This may be computationally expensive and inappropriate for computing complicated topological changes.

The sharpening model (2.2), and hence (2.13), is not written in diffusive (conservative) form and hence it is not a surprise that it leaks mass. When an interface is curved, the amount of ϕ in an interfacial region with value between $0 < \phi < 1/2$ is greater than the amount with value between $1/2 < \phi < 1$, thus more of the phase field gets pushed towards the stable fixed point of $\phi = 0$ than the other stable fixed point of $\phi = 1$ (see Figure 2). Instead of introducing the volume preserving integration step, one may consider developing a conservative sharpening term instead. This can be achieved by embedding the sharpening into the moments of the discrete Boltzmann equation (2.2), specifically the nonequilibrium part of the flux, $\boldsymbol{\psi}^{(1)}$, since we see from (2.7) that the moment equation for ϕ includes the divergence of $\boldsymbol{\psi}$.

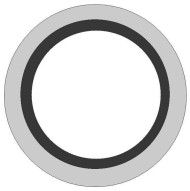

FIG. 2. *Sketch representing the mechanism behind the loss of area. The outer annulus covers a slightly larger area than the inner.*

3. A conservative sharpening scheme. Consider a one-dimensional stationary interface such that (2.13) reduces to

$$\kappa \frac{d^2\phi}{dx^2} + S(\phi) = 0, \tag{3.1}$$

where $\kappa = \lambda\tau$ is the diffusion constant. Solving the above with the boundary conditions $\phi \to 0$ as $x \to -\infty$ and $\phi \to 1$ and $x \to \infty$ yields the interface profile

$$\phi(x) = \frac{1}{1 + e^{-x/L}}, \tag{3.2}$$

where $L = \sqrt{2T\kappa}$ is the lengthscale of the transition region.

Assuming (3.2) holds, we easily calculate the first and second derivatives at the interface to be

$$\frac{d\phi}{dx} = \frac{e^{-x/L}}{L\left(1 + e^{-x/L}\right)^2} = \frac{\phi(1-\phi)}{L}, \tag{3.3}$$

$$\frac{d^2\phi}{dx^2} = \frac{e^{-x/L}\left(e^{-x/L} - 1\right)}{L^2\left(1 + e^{-x/L}\right)^2} = \frac{2\phi(1-\phi)\left(\frac{1}{2} - \phi\right)}{L^2} = \frac{S(\phi)}{\kappa}. \tag{3.4}$$

The term $\phi(1-\phi)$ on the right-hand side of the first equation in (3.3) is the one-dimensional compressive flux of Olsson, Kreiss, and Zahedi [32] and thus we see the connection between the model sharpening term of LeVeque and Yee [29] and the Artificial Compression Method for contact discontinuities [16].

Generalizing to multiple dimensions, we assume the interfacial profile $\phi = \left(1+e^{-n/L}\right)^{-1}$, where $n = |\mathbf{n}|$ and $\mathbf{n} = \nabla\phi/|\nabla\phi|$ is the unit normal vector to the interface. Thus the first and second normal derivatives of the phase field at the interface are

$$\frac{d\phi}{dn} = \nabla\phi\cdot\mathbf{n} = |\nabla\phi| = \frac{\phi(1-\phi)}{L}, \tag{3.5}$$

$$\frac{d^2\phi}{dn^2} = \frac{(\nabla\phi\cdot\nabla)|\nabla\phi|}{|\nabla\phi|} = \frac{2\phi(1-\phi)\left(\frac{1}{2}-\phi\right)}{L^2} = \frac{S(\phi)}{\kappa}. \tag{3.6}$$

The interface curvature can be expressed as

$$C = \nabla\cdot\mathbf{n} = \frac{1}{|\nabla\phi|}\left(\nabla^2\phi - \frac{(\nabla\phi\cdot\nabla)|\nabla\phi|}{|\nabla\phi|}\right). \tag{3.7}$$

This is very convenient for the LBM because it can naturally incorporate into its moments terms written in divergence form.

3.1. The conservative lattice Boltzmann model for interface sharpening. Following section 2 closely, we postulate again the discrete Boltzmann equation (2.2) with all terms defined as before, except for the source term, which becomes

$$R_i = W_i\frac{\phi(1-\phi)}{L\lambda}\mathbf{c}_i\cdot\mathbf{n}. \tag{3.8}$$

Thus, the first two moments of (2.2) are now

$$\partial_t\phi + \partial_\alpha\psi_\alpha = 0, \tag{3.9}$$

$$\partial_t\psi_\alpha + \partial_\beta\Pi_{\alpha\beta} = -\frac{1}{\tau}\left(\psi_\alpha - \psi_\alpha^{(0)}\right) + \frac{\phi(1-\phi)}{L}\mathbf{n}. \tag{3.10}$$

The sharpening term on the right-hand side of (3.10) is similar to the term used in the reinitialization step used in the finite element multidimensional multiphase level set method of Olsson, Kreiss, and Zahedi [32]. Applying the expansion discussed in section 2 and working though the subsequent algebra allows us to find the first correction to the flux,

$$\psi_\alpha^{(1)} = -\left(\lambda\delta_{\alpha\beta} - u_\alpha u_\beta\right)\partial_\beta\phi + \frac{\phi(1-\phi)}{L}\mathbf{n}, \tag{3.11}$$

where we have used the fact that $\psi_\alpha^{(0)} = u_\alpha\phi$ and

$$\partial_{t_0}\psi_\alpha^{(0)} = u_\alpha\partial_t\phi = -u_\alpha\partial_\beta\psi_\beta^{(0)} = -u_\alpha u_\beta\partial_\beta\phi. \tag{3.12}$$

Finally, substituting for $\boldsymbol{\psi} = \boldsymbol{\psi}^{(0)} + \tau\boldsymbol{\psi}^{(1)}$ into the zeroth moment (3.9) and neglecting terms of $\mathcal{O}(\tau^2)$ and $\mathcal{O}(u^2)$ yields the artificial compression interface sharpening equation

$$\frac{\partial\phi}{\partial t} + \mathbf{u}\cdot\nabla\phi = \tau\left(\lambda\nabla^2\phi - \nabla\cdot\frac{\phi(1-\phi)}{L}\mathbf{n}\right). \tag{3.13}$$

Equation (3.13) is similar to the Artificial Compression Model of Olsson, Kreiss, and Zahedi [32]. In the one-dimensional case with initial profile $\phi(x,0) = \phi_0$, where $\phi(x,0)$ is given by (3.2), the compression term vanishes when $L \to L/\lambda$. Thus the second order equation (3.13) becomes the first order transport equation, which has the analytical solution $\phi(x,t) = \phi_0(x-ut)$. That is, the profile simply advects with the flow and remains narrow. We can make similar remarks about the multidimensional case, where the profile is $\phi = (1+e^{-n/L})^{-1}$. The last term of the right-hand side of (3.13), which is responsible for interface sharpening, is

$$\nabla \cdot \left(\frac{\phi(1-\phi)}{L} \mathbf{n} \right) = \frac{\phi(1-\phi)}{L} C + \mathbf{n} \cdot \nabla \frac{\phi(1-\phi)}{L}, \tag{3.14}$$

where $C = \nabla \cdot \mathbf{n}$ is the interface curvature. From (3.5), (3.6), and (3.7), we see that

$$\frac{\phi(1-\phi)}{L} C = \left(\nabla^2 \phi - \frac{(\nabla\phi \cdot \nabla)|\nabla\phi|}{|\nabla\phi|} \right), \tag{3.15}$$

$$\mathbf{n} \cdot \nabla \frac{\phi(1-\phi)}{L} = \frac{(\nabla\phi \cdot \nabla)|\nabla\phi|}{|\nabla\phi|}, \tag{3.16}$$

and hence the sharpening term is an antidiffusive term that acts to counteract diffusion and maintain narrow phase boundaries. Furthermore, with the interface normal defined to be $\mathbf{n} = \nabla\phi/|\nabla\phi|$, the diffusion term can be written as $\nabla \cdot ((\nabla\phi \cdot \mathbf{n}))\mathbf{n}$ and thus the right-hand side of (3.13) as

$$\kappa \nabla^2 \phi - \tau \nabla \cdot \frac{\phi(1-\phi)}{L} \mathbf{n} = \tau \nabla \cdot \left(\lambda (\nabla\phi \cdot \mathbf{n}) \mathbf{n} - \nabla \cdot \frac{\phi(1-\phi)}{L} \mathbf{n} \right). \tag{3.17}$$

This shows, as remarked by Olsson, Kreiss, and Zahedi [32], the diffusion causes a flux in the direction of the interface normal only, and this becomes balanced by the compressive flux term $\nabla \cdot \phi(1-\phi)\mathbf{n}$. If L in the compression term in (3.13) is transformed to $L \to L/\lambda$ and the initial profile $\phi_0 = (1+e^{-n/L})^{-1}$, then the solution to (3.13) is again the sharp travelling wave solution.

3.2. Implementation. We implement the two-relaxation-time (TRT) form of the lattice Boltzmann algorithm, which splits the collision and source terms into their odd and even constituents (in terms of the order of $\mathbf{c}_i$). This relaxes the odd and even moments of the discrete Boltzmann equation (2.2) at different rates. The TRT discrete Boltzmann equation may be written as

$$\partial_t f_i + c_{i\alpha} \partial_\alpha f_i = -\frac{1}{\tau^+} \left(\frac{1}{2}(f_i + f_j) - f_i^{(0+)} \right) - \frac{1}{\tau^-} \left(\frac{1}{2}(f_i - f_j) - f_i^{(0-)} \right), \tag{3.18}$$

where we have defined $f_i^{(0+)} = W_i \phi$ and $f_i^{(0-)} = \lambda^{-1} \mathbf{c}_i \cdot \mathbf{u} + \tau^- R_i$. In the above, j is in the opposite direction of i such that $\mathbf{c}_j = -\mathbf{c}_i$. The TRT scheme reduces to the standard single relaxation time BGK model (2.2) when $\tau^+ = \tau^- = \tau$.

To derive a lattice Boltzmann algorithm we integrate (2.2) along a characteristic for time Δt to give

$$f_i(\mathbf{x} + \mathbf{c}\Delta t, t + \Delta t) - f_i(\mathbf{x}, t) = \int_0^{\Delta t} \Omega_i(\mathbf{x} + \mathbf{c}_i s, t + s) ds, \tag{3.19}$$

where Ω_i represents the right-hand side of (3.18). The integral on the right hand side of (3.19) can be approximated with the trapezium rule to yield the implicit system of equations

$$f_i(\mathbf{x}+\mathbf{c}_i\Delta t, t+\Delta t)-f_i(\mathbf{x},t)=\frac{\Delta t}{2}\Big(\Omega_i(\mathbf{x}+\mathbf{c}_i\Delta t, t+\Delta t) + \Omega_i(\mathbf{x},t)\Big)+\mathcal{O}\left(\Delta t^3\right). \tag{3.20}$$

Following He, Cen, and Zhang [17] we remove this implicitness by introducing the new variable

$$\bar{f}_i = f_i - \frac{\Delta t}{2\tau}\left(f_i - f_i^{(0)}\right) - \frac{\Delta t}{2}R_i. \tag{3.21}$$

We can now discard f_i and evolve $\bar{f}_i$ according to

$$\begin{aligned}\overline{f}_i(\mathbf{x}+\mathbf{c}_i, t+\Delta t) - \overline{f}_i(\mathbf{x},t) = &-\frac{\Delta t}{\tau^+ + \Delta t/2}\left(\frac{1}{2}\left(\overline{f}_i + \overline{f}_j\right) - f_i^{(0+)}\right)\\ &- \frac{\Delta t}{\tau^- + \Delta t/2}\left(\frac{1}{2}\left(\overline{f}_i - \overline{f}_j\right) - f_i^{(0-)}.\right)\end{aligned} \tag{3.22}$$

The motivation for using TRT is its enhanced numerical stability at very little additional computational cost. The diffusion is now set by the odd relation time, $\kappa = \lambda\tau^-$, while the even relaxation time is essentially a free parameter that is set according to numerical considerations. It is well known that there are numerically favorable choices of the so-called "magic parameter" $\Lambda = \tau^+\tau^-$ [10]. We choose $\Lambda = 1/4$ since it has been shown to offer optimal stability. Other sensible choices that are not under investigation here are $\Lambda = 1/6$, which removes a fourth order diffusion error, and $\Lambda = 1/12$, which removes a third order advection error [21].

The gradients in (3.8), which are included in the odd equilibria $f_i^{(0-)}$ in the algorithm (3.22), need to be computed using finite differences. The directional derivatives and gradients are approximated using

$$\mathbf{c}_i \cdot \nabla\phi \approx \frac{\phi(\mathbf{x}+\mathbf{c}_i, t) - \phi(\mathbf{x}-\mathbf{c}_i\Delta t, t)}{2\Delta t}, \tag{3.23}$$

$$\nabla\phi \approx \sum_i \frac{\lambda W_i\left(\phi(\mathbf{x}+\mathbf{c}_i, t) - \phi(\mathbf{x}-\mathbf{c}_i\Delta t, t)\right)}{2\Delta t}, \tag{3.24}$$

respectively, and the source term is applied everywhere where $\nabla\phi > 0$. We do not consider other finite difference formulae for the computation of derivatives on the lattice.

4. Numerical simulations. In all simulations that follow, the grid spacing is $\Delta x = 1/m$, where m is the number of grid points in a characteristic length and the timestep is $\Delta t = 0.1\Delta x$. The sharpening length L is set to either Δx or $2\Delta x$. Furthermore, in all tests below the flow velocity $\mathbf{u}$ is imposed, and not derived nor computed from another solver.

4.1. One-dimensional results. For simplicity we use D1Q2 lattice with one lattice velocity pointing in positive direction (c_1) and another (c_2) in the negative. The weights are $W_1 = W_2$=1/2 and $\lambda = 1$ in so-called lattice units with $\Delta x = \Delta t = 1$. We first consider the case of no advection, $u = 0$, and monitor the sharpening of the

initially diffuse profile $\phi(0) = \sin \pi x^2$ when the nondimensional diffusion coefficient (analogous to the Péclet number) is 0.1. The number of grid points is 100 and $L = 1$ in lattice units. Figure 3 plots the evolution of at $t = 0.0$, 0.01, and 0.1. The phase boundary is shown to quickly sharpen to a narrow interface of about four nodes.

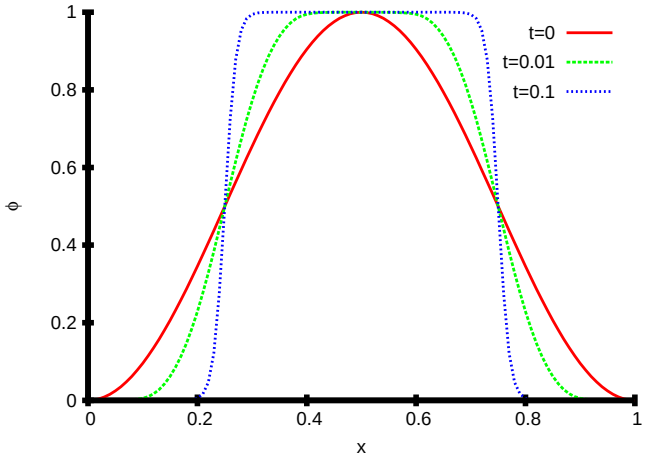

FIG. 3. *Plot showing the sharpening of the phase field using the antidiffusive lattice Boltzmann formation on the D1Q2 lattice with $L = 1$ in lattice units.*

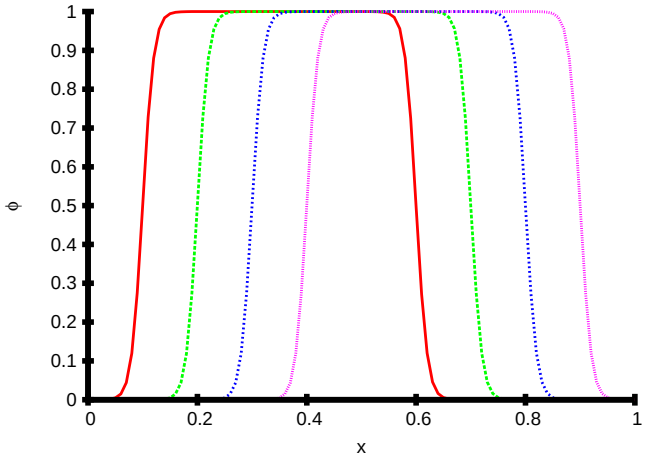

FIG. 4. *The advection and sharpening of the phase field using the antidiffusive lattice Boltzmann formation on a D1Q2 lattice with $L = 1$ in lattice units. Plots are taken at times $t = 0.1, 0.2, 0.3, 0.4$.*

Figure 4 shows the advection of the phase field with initial profile $\phi = (1 + \tanh(5 \sin 2\pi x))$ and a constant velocity $u = 1$ (or $u = 0.1$ in lattice units). The parameters are the same as the previous simulation. The profile propagates correctly with the advection velocity in both cases and again sharpens very quickly. There is no lattice pinning at all, even though we have very narrow transition regions.

4.2. Two-dimensional results. We use the D2Q9 lattice for all two-dimensional simulations. This lattice is shown in Figure 1 and has weights $W_0 = 4/9$, $W_{1,2,3,4} =$

1/9, and $W_{5,6,7,8} = 1/36$. The constant $\lambda = 3$ in lattice units. The simpler 4-point D2Q4 and 5-point D2Q5 lattices have enough independent moments to recover the target equation (3.13), and will have computational advantages in terms of efficiency, but the D2Q9 model is chosen here because of its widespread use and its larger stencil for computing finite difference approximations to $\mathbf{n}$. In all simulations the nondimensional diffusion coefficient was set to 0.003.

4.2.1. Advecting drop. The first test is an advecting circular patch of fluid of radius 0.15 in a square domain of side 1. The center of the patch is initially positioned at (0.25, 0.25) with $\phi = 1$ inside and $\phi = 0$ outside. The imposed velocity is $\mathbf{u} = (1, 1)$. The number of grid points in each direction is 100 and $L = 1$ in lattice units. Shown in Figure 5 is the transport of the circular patch at $t = 0.1, 0.2, 0.3,$ and 0.4. Its center at the final time is at position (0.65,0.65) and thus shown to advect at the correct (imposed) velocity. Volume (total ϕ) is conserved to machine precision. The interface, which is initially completely sharp, diffuses slightly during the first timesteps, and the final phase boundary is very narrow—just three grid points wide—but a little distortion is observed.

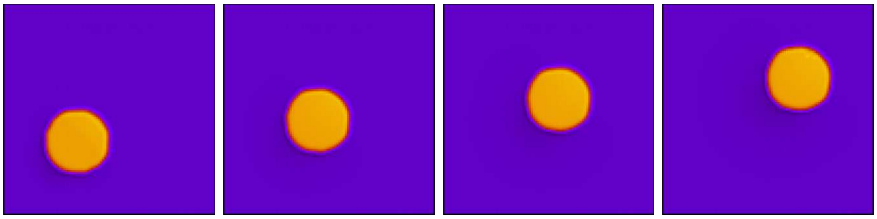

FIG. 5. *Advecting circular patch using the antidiffusive lattice Boltzmann formation. Plots are taken at times (from left to right)* $t = 0.1, 0.2, 0.3, 0.4$.

This distortion and the interface width is seen more clearly in the graph on the left of Figure 6, which plots the phase filed ϕ against the radius of the patch from its center. The plot on the right of Figure 6 shows the radius from the center when the spatial resolution is doubled. In this instance the interface remains very narrow and almost completely free of any facetting.

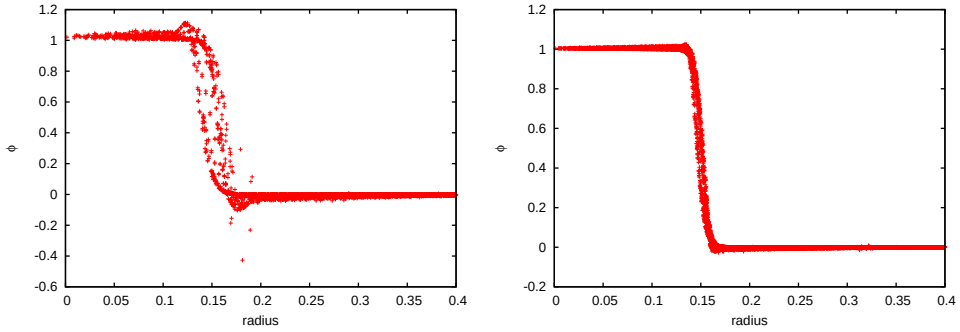

FIG. 6. *Plot of ϕ against the radius of the drop from its center on a* 100×100 *(left) and a* 200×200 *(right) grid with* $L = 1$.

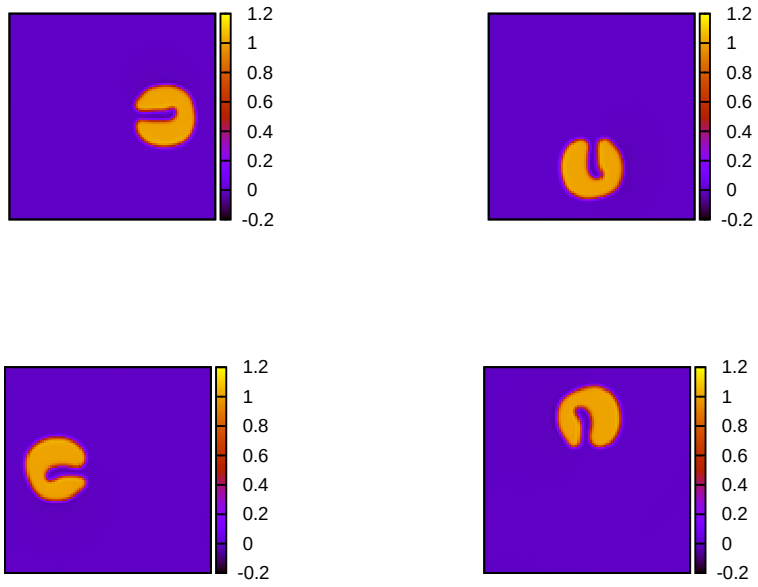

FIG. 7. *Plot after (from left to right) a quarter, half, three quarters, and a full rotation of Zalesak's slotted disk test using the antidiffusive lattice Boltzmann formation. The domain size is* 100×100 *grid points and* $L = 1$.

4.2.2. Zalesak's slotted disk. The next test is Zalesak's slotted disk [53]. A disk of radius 0.15 with a slot of height 0.05 is centerd at position (0.5,0.75) in a square box of side 1. Within the slotted disk, $\phi = 1$ and elsewhere $\phi = 0$. The disk is rotated about the center of the domain with velocity $\mathbf{u} = (2y - 1, -2x + 1)$. Figure 7 plots the phase field after 1/4, 1/2, 3/4 of a rotation, and a full rotation, on a grid of size 100×100 and $L = 1$ in lattice units. Volume is conserved to 13 decimal places but although the shape is recognizable after a full rotation, it has distorted considerably.

Doubling the resolution with the same L allows the disk to return to its initial position with its shape preserved very well, as shown in Figure 8. The corners of the slot have become smeared during the LBM simulation and some small numerical discrepancies can be noticed in Figure 8. These may be improved by higher order approximations to the gradients in R_i, increased resolution, or larger L, but these are not investigated further here. Still, the disk returns to its initial position with its shape well preserved and the smearing of corners is common in all diffusive interface capturing methods [47]. The interface remains sharp (three grid points wide) with little smearing away from the corners and volume is again conserved to 13 decimal places.

4.2.3. Time-reversed vortex field. The final test of the proposed method is the stringent circular interface in the time-reversed vortex field [28]. A circular patch of radius 0.15 is placed in a domain of side 1 with its center at (0.5,0.75) and subjected

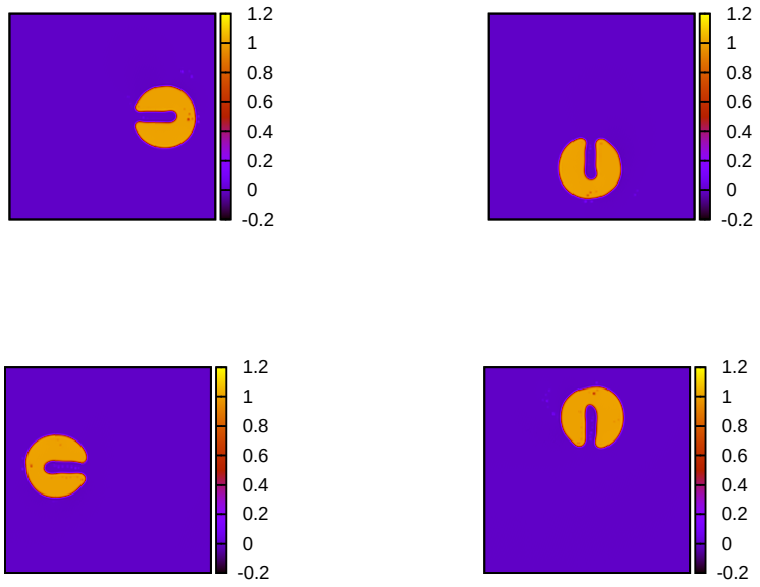

FIG. 8. *Plot after (from left to right) a quarter, half, three quarters, and a full rotation of Zalesak's slotted disk test using the antidiffusive lattice Boltzmann formation. The domain size is* 200×200 *grid points and* $L = 1$.

to the velocity field

$$u(x, y, t) = \cos\left(\frac{\pi t}{T}\right) \sin^2(\pi x) \sin(2\pi y), \tag{4.1}$$

$$v(x, y, t) = -\cos\left(\frac{\pi t}{T}\right) \sin^2(\pi y) \sin(2\pi x), \tag{4.2}$$

where the constant T is the time-reversal period. This imposed velocity $\mathbf{u}$ is a vortex field that stretches the phase boundary of ϕ into long spirally filaments about the center of the domain. The temporal term $\cos(\pi t/T)$ causes the flow to reverse and the phase field ϕ to return to its initial state at $t = T$. The maximum distortion of the phase field is when $t = T/2$ and the longer the period T, the more stretched and distorted ϕ will become.

Figure 9 plots the phase field at times $t = 0.5$, 1, 1.5, and 2 with period $T = 2$ in a domain of size 100×100. The sharpening length is $L = 1$ in lattice units. The stretching of ϕ until $t = 1$ and its attempted return to the circle is evident. Volume is again preserved to 13 decimal places but some facetting is observed. The center of the patch at $t = 2$ is calculated to be (0.5, 0.76), so it as departed only by one grid point in the vertical direction from its started position.

The effect of doubling the resolution and L is shown in Figure 10. The center of the patch at $t = 2$ is now (0.5, 0.75), i.e., the same as its starting position, and the final shape is an almost perfect circle. If we set $L = 1$ with this resolution we

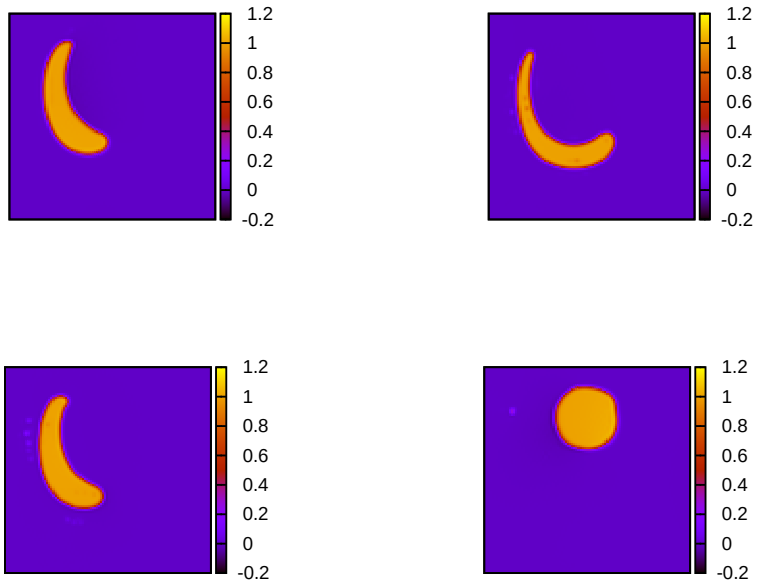

FIG. 9. *Plots of the vortex reversal test problem at time (from left to right)* $t = 0.5$, 1, 1.5, *and* 2 *with* $T = 2$ *using the antidiffusive lattice Boltzmann model. The domain size is* 100×100 *grid points and* $L = 1$.

can compute an extremely narrow interface but numerical inaccuracies are observed within the phase field, as shown in Figure 11. To offer clarification we plot in Figure 12 ϕ against the radius of the patch from its center after one full reversal with 200×200 grid points when $L = 1$ (left) and $L = 2$. We can see that the interface is narrow and almost perfectly circular when $L = 2$ and extremely thin when $L = 1$, but this excessive sharpening comes at the price of spurious numerical results away from the center of patch. This is due to the coarse resolution for computing the approximations to the gradients of ϕ is the unit normal, $\mathbf{n}$. By doubling the resolution again we decrease these numerical errors significantly, as shown in Figure 13.

Figure 14 plots the temporal development of an initially circular patch of fluid in the vortex field when the period is $T = 6$. Snapshots are taken at time $t = 1$, 2, 3, and 6. The spatial resolution is 400×400 and the sharpening parameter is $L = 2$ in lattice units. Severe stretching is observed but the filament keeps its integrity quite well at the maximum distortion. The patch returns to its initial state although the final shape has suffered some distortions and roughness to its narrow interface (Figure 15). Increasing the period still further to $T = 8$ produces extreme stretching but nevertheless the LBM captures the distortions and maintains narrow interfaces without a loss of volume. Some numerical instabilities are observed at the maximum stretch where the filament breaks at the trailing corner, producing errors to the final circle upon flow reversal, as shown in Figure 16.

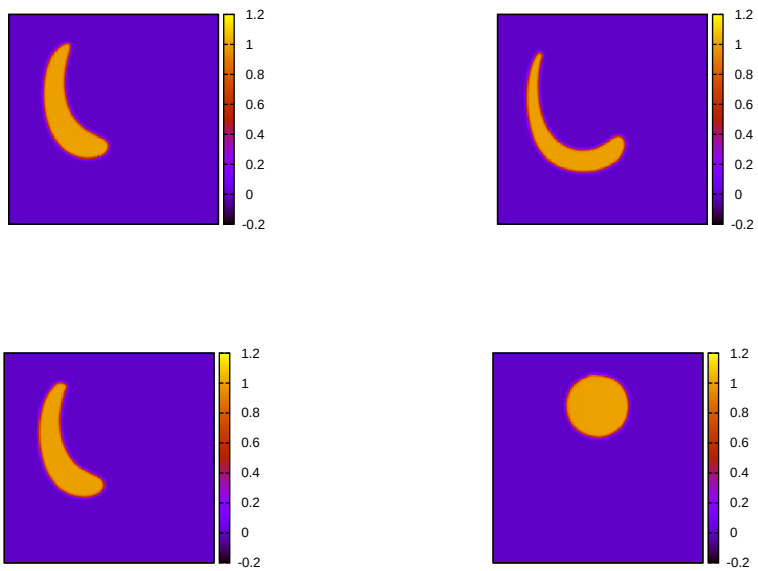

FIG. 10. *Plots of the vortex reversal test problem at times (from left to right)* $t = 0.5$, 1, 1.5, *and* 2 *with* $T = 2$ *using the antidiffusive lattice Boltzmann model. The domain size is* 200×200 *grid points and* $L = 2$.

5. Conclusion. We have presented a conservative lattice Boltzmann model for the advection and sharpening of interfaces that commonly arise in applications such as multiphase flow. The method was developed by writing in one dimension the algebraic sharpening source term of LeVeque and Yee [29], and hence the LBM of Reis and Dellar [37], in divergence form. In multiple dimensions the antidiffusion term responsible for sharpening acts in the direction normal to the interface and the model is very similar to the the Artificial Compression Method of Olsson, Kreiss, and Zahedi [32]. Classic benchmark tests for interface capturing methods have been performed in one and two dimensions and the method has been shown to compute narrow interfaces on reasonable meshes without any loss of volume. These included stringent tests with significant deformation. The proposed model has been shown to capture the changes in interface topology very well, even in quite extreme flow fields. Zalesak's slotted disk proved to be the most difficult for the model, which was to be expected since the diffusion term in the model smears sharp corners. Indeed, sharp corners cause numerical instabilities in diffuse interface capturing methods but the new method proposed here performs very well in terms of mass loss error and the final shape when compared with many existing (nonlattice-Boltzmann) interface sharpening methods [47]. The vortex reversal test can cause volume loss and numerical instabilities with sharpening algorithms for diffuse interface models, as discussed by Sun and Beckermann [47]. Even level set methods require nondiffusive methods such as MacCormack, or high order schemes like WENO-5 to accurately compute this test [41]. However, the results of the vortex test with the antidiffusive lattice Boltzmann method showed no loss of volume and in the cases when $T = 2$ and $T = 6$ showed very few numerical

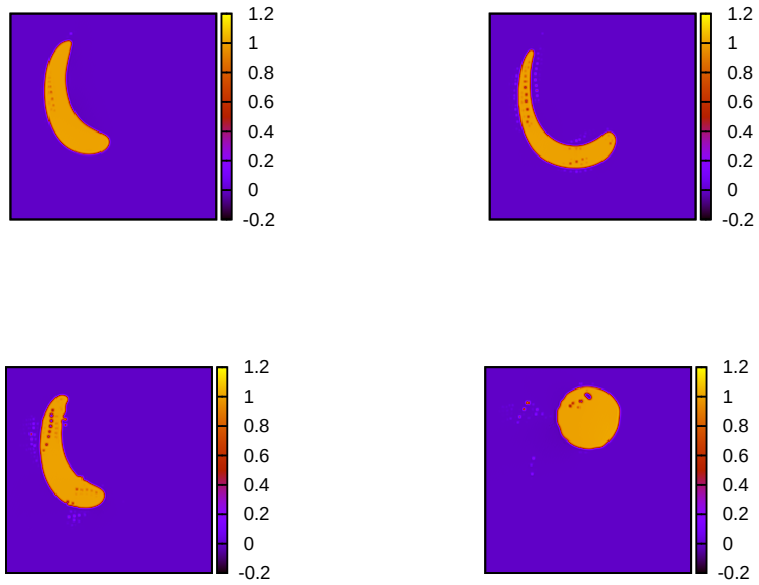

FIG. 11. *Plots of the vortex reversal test problem at times (from left to right)* $t = 0.5$, 1, 1.5, *and* 2 *with* $T = 2$ *using the antidiffusive lattice Boltzmann model. The domain size is* 200×200 *grid points and* $L = 1$.

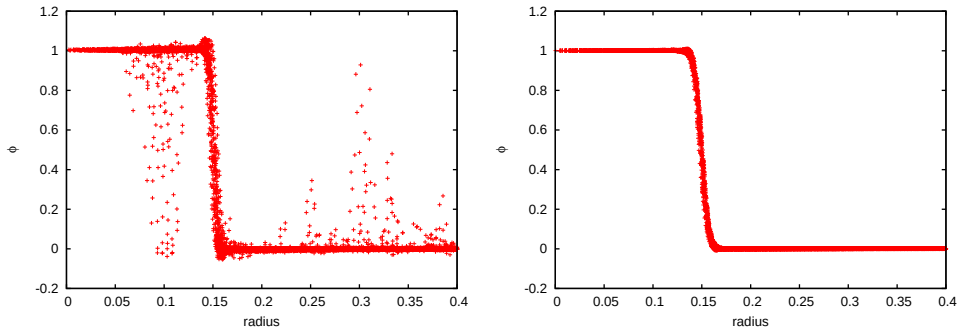

FIG. 12. *Plot of* ϕ *against the radius of the patch from its center after one full reversal of the vortex test when* $L = 1$ *(left) and* $L = 2$ *(right). The grid size is* 200×200.

instabilities in the used parameter range, allowing the circle to be restored after the deformation is reversed. Some errors are observed in the extreme case of $T = 8$ but even here the final state is recognizable. Optimal values for the parameter L have not been formally determined here but $1 \leq L \leq 2$ has been sufficient for the tests we performed (or in units of grid spacing, $\Delta x \leq L \leq 2\Delta x$). Our model may be adopted and combined with multiphase lattice Boltzmann models, e.g., to replace the ad-hoc recoloring step in color gradient models and to prevent the smearing of transition regions. The methodology also provides a quantitative approach to the determination

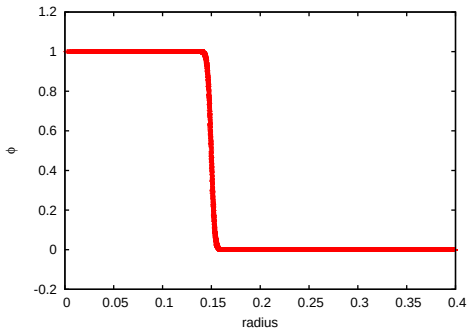

FIG. 13. *Plot of ϕ against the radius of the patch from its center after one full reversal of the vortex test when $L = 2$ and the grid size is 400×400.*

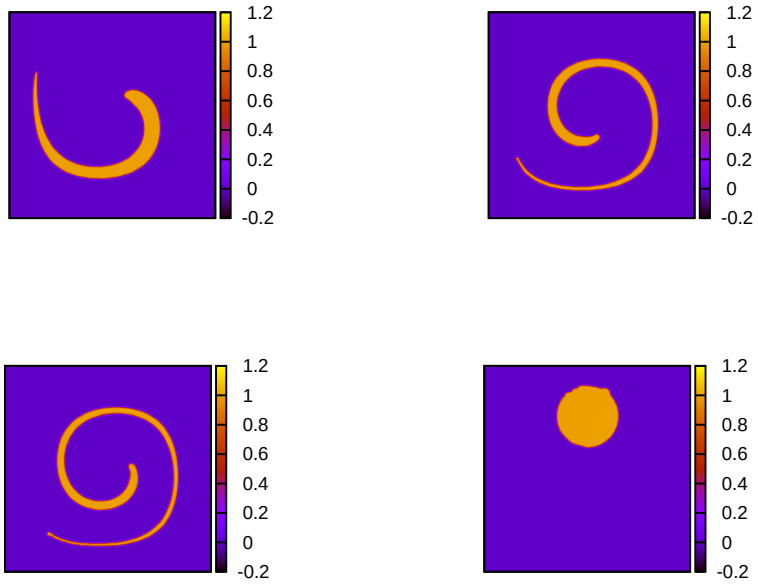

FIG. 14. *Plots of the vortex reversal test problem at times $t = 1$, 2, 3, and 6 with $T = 6$ using the antidiffusive lattice Boltzmann model. The domain size is 400×400 grid points and $L = 2$.*

of the interface advection, free from the mass conservation troubles discussed in other approaches [37, 41, 47]. It must be emphasized again that the velocity field in all of the simulations presented here was *imposed* and one would naturally expect additional numerical errors when the algorithm is coupled to a solver for the flow field. Compressibility and Galilean invariance errors of the LBM might distort the phase field behavior (note from subsection 3.1 that a spatially and temporally dependent velocity field may introduce further artefacts) and a very narrow interface profile with few grid points in the transition region could lead to a noisier pressure profile across the interface (especially when the density ratio is large). In addition, the potential

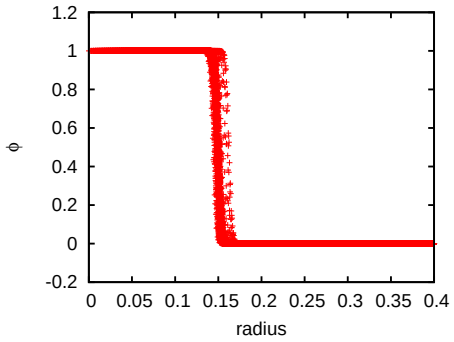

FIG. 15. *Plot of ϕ against the radius of the patch from its center after one full reversal of the vortex test when $L = 6$ and the grid size is 400×400.*

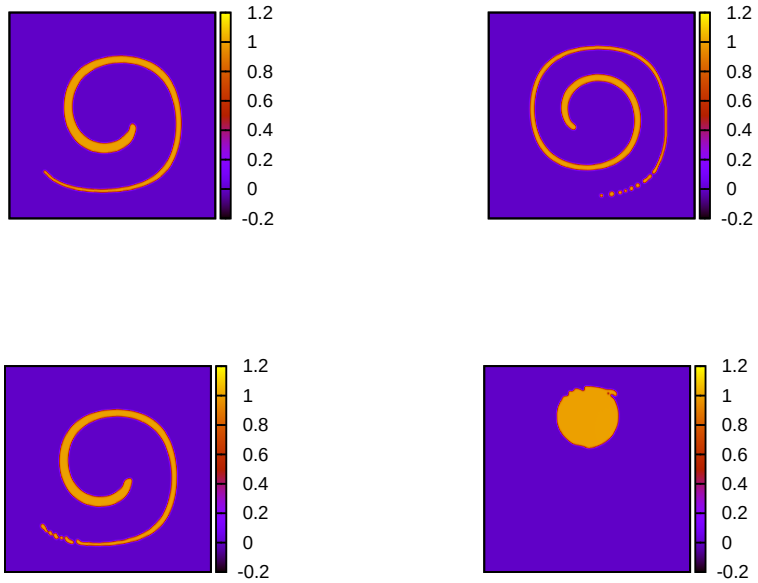

FIG. 16. *Plots of the vortex reversal test problem at times $t = 2$, 4, 6, and 8 with $T = 8$ using the antidiffusive lattice Boltzmann model. The domain size is 400×400 grid points and $L = 2$.*

for a fully coupled solver to generate spurious microcurrents and distort an interface in the narrow limit could be a concern. These remain interesting and important discussions, with further research clearly needed. Still, the method presented here offers insight into lattice Boltzmann interface advection-sharpening algorithms and may help future surface tension models capture interfacial kinematics without lattice pinning and without the need for excessive resolution.

REFERENCES

[1] C. K. Aidun and J. R. Clausen, *Lattice Boltzmann method for complex flows*, Annu. Rev. Fluid Mech., 42 (2010), pp. 439–472, https://doi.org/10.1146/annurev-fluid-121108-145519.

[2] D. Anderson, G. McFadden, and A. A. Wheeler, *Diffuse-interface methods in fluid mechanics*, Annu. Rev. Fluid Mech., 30 (1998), pp. 139–165, https://doi.org/10.1146/annurev.fluid.30.1.139.

[3] W. Bao and S. Jin, *The random projection method for hyperbolic conservation laws with stiff reaction terms*, J. Comput. Phys., 163 (2000), pp. 216–248, https://doi.org/10.1006/jcph.2000.6572.

[4] L. Chen, Q. Kang, Y. Mu, Y. He, and W. Tao, *A critical review of the pseudopotential multiphase lattice Boltzmann model: Methods and applications*, Int. J. Heat Mass Trans., 76 (2014), pp. 210–236, https://doi.org/10.1016/j.ijheatmasstransfer.2014.04.032.

[5] A. Chiapolino, R. Saurel, and B. Nkonga, *Sharpening diffuse interfaces with compressible fluids on unstructured meshes*, J. Comput. Phys., 340 (2017), pp. 389–417, https://doi.org/10.1016/j.jcp.2017.03.042.

[6] A. Chorin, *Random choice solution of hyperbolic systems*, J. Comput. Phys., 22 (1976), pp. 517–533, https://doi.org/10.1016/0021-9991(76)90047-4.

[7] P. Colella, *Volume-of-fluid methods for partial differential equations*, Kluwer/Plenum, New York, 2001, pp. 161–177, https://doi.org/10.1007/978-1-4615-0663-8_17.

[8] P. Colella, A. Majda, and V. Roytburd, *Theoretical and numerical structure for reacting shock waves*, SIAM J. Sci. Statist. Comput., 7 (1986), pp. 1059–1080, https://doi.org/10.1137/0907073.

[9] R. Folch, A. Casademunt, A. Hernàndez-Machado, and L. Ramirez-Piscina, *A phase-field model for Hele-Shaw flows with arbitrary viscosity contrast.* 1. *Theoretical approach*, Phys. Rev. E, 60 (1999), 1724, https://doi.org/10.1103/PhysRevE.60.1724.

[10] I. Ginzburg, *Equilibrium-type and link-type lattice Boltzmann models for generic advection and anisotropic-dispersion equation*, Adv. Water Resour., 28 (2005), pp. 1171–1195, https://doi.org/10.1016/j.advwatres.2005.03.004.

[11] D. Grunau, S. Chen, and K. Eggert, *A lattice Boltzmann model for multiphase flow*, Phys Fluids A, 5 (1993), pp. 2557–2561, https://doi.org/10.1063/1.858769.

[12] A. K. Gunstensen and D. H. Rothman, *Lattice-Boltzmann studies of immiscible two-phase flow through porous media*, J. Geophys. Res.: Solid Earth, 98 (1993), pp. 6431–6441, https://doi.org/10.1029/92JB02660.

[13] Z. Guo, C. Zheng, and B. Shi, *Discrete lattice effects on the forcing term in the lattice Boltzmann method*, Phys. Rev. E, 65 (2002), 046308, https://doi.org/10.1103/PhysRevE.65.046308.

[14] I. Halliday, A. Hollis, and C. Care, *Lattice Boltzmann algorithm for continuum multicomponent flow*, Phys. Rev. E, 76 (2007), 026708, https://doi.org/10.1103/PhysRevE.76.026708.

[15] I. Halliday, S. Lishchuk, T. Spencer, G. Ponterelli, and C. Care, *Multi-component lattice Boltzmann equation for fluid-filled vesicles in flow*, Phys. Rev. E., 87 (2013), 023307, https://doi.org/10.1103/PhysRevE.87.023307.

[16] A. Harten, *The artificial compression method for computation of shocks and contact discontinuities.* 1. *Single conservation laws*, Commun. Pure Appl. Math., (1977), pp. 611–638, https://doi.org/10.1002/cpa.3160300506.

[17] X. He, C. Chen, and R. Zhang, *A lattice Boltzmann scheme for incompressible multiphase flow and its application in simulation of Rayleigh-Taylor instability*, J. Comput. Phys., 152 (1999), pp. 642–663, https://doi.org/10.1006/jcph.1999.6257.

[18] C. Hirt and B. Nichols, *Volume of fluid (VoF) method for the dynamics of free boundaries*, J. Comput. Phys., 39 (1981), pp. 201–225, https://doi.org/10.1.1.413.7358.

[19] H. Huang, M. Sukop, and X. Lu, *Multiphase Lattice Boltzmann Methods: Theory and Application*, John Wiley & Sons, New York, 2015, https://doi.org/10.1002/9781118971451.

[20] H. Huang, X.-Y. Wang, and L. Lu, *Evaluation of three lattice Boltzmann models for multiphase flows in porous media*, Comput. Math. Appl., 61 (2011), pp. 3606–3617, https://doi.org/10.1016/j.camwa.2010.06.034.

[21] D. d'Humières and I. Ginzburg, *Viscosity independent numerical errors for lattice Boltzmann models: From recurrence equations to "magic" collision numbers*, Comput. Math. Appl., 58 (2009), pp. 823–840, https://doi.org/10.1016/j.camwa.2009.02.008.

[22] T. Inamuro, N. Konishi, and F. Ogino, *A Galilean invariant model of the lattice Boltzmann method for multiphase fluid flows using free-energy approach*, Comput. Phys. Comm., 129 (2000), pp. 32–45, https://doi.org/10.1016/S0010-4655(00)00090-4.

[23] P. Lallemand, L.-S. Luo, and Y. Peng, *A lattice Boltzmann front-tracking method for interface dynamics with surface tension in two dimensions*, J. Comput. Phys., 226 (2007), pp. 1367–1384, https://doi.org/10.1016/j.cp.2007.05.021.

[24] M. Latva-Kokko and D. H. Rothman, *Diffusion properties of gradient-based lattice Boltzmann models of immiscible fluids*, Phys. Rev. E, 71 (2005), 056702, https://doi.org/10.1103/PhysRevE.71.056702.

[25] S. Leclaire, A. Parmigiani, O. Malaspinas, B. Chopard, and J. Latt, *Generalized three-dimensional lattice Boltzmann color-gradient method for immiscible two-phase pore-scale imbibition and drainage in porous media*, Phys. Rev. E, 95 (2017), 033306, https://doi.org/10.1103/PhysRevE.95.033306.

[26] T. Lee and P. Fischer, *Eliminating parasitic currents in the lattice Boltzmann equation method for nonideal gases*, Phys. Rev. E, 74 (2006), 046709, https://doi.org/10.1103/PhysRevE.74.046709.

[27] T. Lee and C. Lin, *A stable discretization of the lattice Boltzmann equation for simulation of incompressible two-phase flows at high density ratio*, J. Comput. Phys., 206 (2005), pp. 16–47, https://doi.org/10.1016/j.jcp.2004.12.001.

[28] R. J. LeVeque and Z. Li, *The immersed interface methods for elliptic equations with discontinuous coefficients and singular sources*, SIAM J. Numer. Anal., 31 (1994), pp. 1019–1044, https://doi.org/10.1137/0731054.

[29] R. LeVeque and H. C. Yee, *A study of numerical methods for hyperbolic conservation laws with stiff source terms*, J. Comput. Phys., 86 (1990), pp. 187–210, https://doi.org/10.1016/0021-9991(90)90097-K.

[30] S. Lishchuk, C. Care, and I. Halliday, *Lattice Boltzmann algorithm for surface tension with greatly reduced microcurrents*, Phys. Rev. E, 67 (2003), 036701, https://doi.org/10.1103/PhysRevE.67.036701.

[31] H. Liu, Q. Kang, C. R. Leonardi, S. Schmieschek, A. Narváez, B. Jones, J. R. Williams, A. J. Valocchi, and J. Harting, *Multiphase lattice Boltzmann simulations for porous media applications*, Comput. Geosci., 20 (2016), pp. 777–805, https://doi.org/10.1007/s10596-015-9542-3.

[32] E. Olsson, G. Kreiss, and S. Zahedi, *A conservative level set method for two phase flow* II, J. Comput. Phys., 225 (2007), pp. 785–807, https://doi.org/10.1016/j.jcp.2006.12.027.

[33] S. Osher and J. A. Sethian, *Fronts propagating with curvature-dependent speed: algorithms based on Hamilton-Jacobi formulations*, J. Comput. Phys., 79 (1988), pp. 12–49, https://doi.org/10.1016/0021-9991(88)90002-2.

[34] R. B. Pember, *Numerical methods for hyperbolic conservation laws with stiff relaxation* 1. *Spurious solutions*, SIAM J. Appl. Math., 53 (1993), pp. 1293–1330, https://doi.org/10.1137/0153062.

[35] G. Pereira, *A multiphase single relaxation time lattice Boltzmann model for heterogeneous porous media*, Appl. Math. Model., 44 (2017), pp. 160–174, https://doi.org/10.1016/j.apm.2016.11.009.

[36] C. Pooley and K. Furtado, *Eliminating spurious velocities in the free-energy lattice Boltzmann method*, Phys. Rev. E, 77 (2008), 046702, https://doi.org/0.1103/PhysRevE.77.046702.

[37] T. Reis and P. Dellar, *A volume-preserving sharpening approach for the propagation of sharp phase boundaries in multiphase lattice Boltzmann simulations*, Comput. Fluid., 46 (2011), pp. 417–421, https://doi.org/10.1016/j.compfluid.2010.12.005.

[38] T. Reis and T. Phillips, *Lattice Boltzmann model for simulating immiscible two-phase flows*, J. Phys. A, 40 (2007), p. 4033, https://doi.org/10.1088/1751-8113/40/14/018.

[39] D. H. Rothman and J. M. Keller, *Immiscible cellular-automaton fluids*, J. Stat. Phys., 52 (1988), pp. 1119–1127, https://doi.org/10.1007/BF01019743.

[40] R. Sadeghi, M. Shadloo, M. Hopp-Hirschler, A. Hadjadj, and U. Nieken, *Three-dimensional lattice Boltzmann simulations of high density ratio two-phase flows in porous media*, Comput. Math. Appl., 75 (2018), pp. 2445–2465, https://doi.org/https://doi.org/10.1016/j.camwa.2017.12.028.

[41] A. Salih and M. S. Ghosh, *Some numerical studies of interface advection properties of level set method*, Sadhana, 34 (2009), pp. 271–298, https://doi.org/10.1007/s12046-009-0013-1.

[42] J. A. Sethian, *Level Set Methods and Fast Marching Methods: Evolving Interfaces in Computational Geometry, Fluid Mechanics, Computer Vision, and Materials Science*, Vol. 3, Cambridge University Press, Cambridge, UK, 1999, https://doi.org/10.1108/k.2000.29.2.

239.3.
[43] J. Sethian and P. Smereka, *Level set methods for fluid interfaces*, Annu. Rev. Fluid Mech., 35 (2003), pp. 341–372, https://doi.org/10.1146/annurev.fluid.35.101101.161105.
[44] X. Shan and H. Chen, *Lattice Boltzmann model for simulating flows with multiple phases and components*, Phys. Rev. E, 47 (1993), 1815, https://doi.org/10.1103/PhysRevE.47.1815.
[45] K. So, X. Hu, and N. Adams, *Anti-diffusion interface sharpening technique for two-phase compressible flow simulations*, J. Comput. Phys., 231 (2012), pp. 4304–4323, https://doi.org/10.1016/j.jcp.2012.02.013.
[46] T. Spencer and I. Halliday, *Multicomponent lattice Boltzmann equation method with a discontinuous hydrodynamic interface*, Phys. Rev. E., 88 (2013), 063305, https://doi.org/10.1103/PhysRevE.88.063305.
[47] Y. Sun and C. Beckermann, *Sharp interface tracking using the phase-field equation*, J. Comput. Phys., 220 (2007), pp. 626–653, https://doi.org/10.1016/j.jcp.2006.05.025.
[48] M. R. Swift, W. Osborn, and J. Yeomans, *Lattice Boltzmann simulation of nonideal fluids*, Phys. Rev. Lett., 75 (1995), pp. 830–833, https://doi.org/10.1103/PhysRevLett.75.830.
[49] A. Tiwari, J. B. Freund, and C. Pantano, *A diffuse interface model with immiscibility preservation*, J. Comput. Phys., 252 (2013), pp. 290–309, https://doi.org/10.1016/j.jcp.2013.06.021.
[50] J. Tölke, M. Krafczyk, M. Schultz, and E. Rank, *Lattice Boltzmann simulations of binary fluid flow through porous media*, R. Soc. Lond. Philos. Trans. Ser. A Math. Phys. Eng. Sci., 360 (2002), pp. 535–545, https://doi.org/10.1098/rsta.2001.0944.
[51] Z. Xu, H. Liu, and A. J. Valocchi, *Lattice Boltzmann simulation of immiscible two-phase flow with capillary valve effect in porous media*, Water Resour. Res., 53 (2017), pp. 3770–3790, https://doi.org/10.1002/2017WR020373.
[52] D. Youngs, *Time-dependent multi-material flow with large fluid distortion*, in Numerical Methods for Fluid Dynamics, K. W. Morton and M. J. Baines, eds., Academic Press, New York, 1982, pp. 273–285.
[53] S. Zalesak, *Fully multidimensional flux-corrected transport algorithms for fluids*, J. Comput. Phys., 31 (1979), pp. 335–362, https://doi.org/10.1016/0021-9991(79)90051-2.